Microfluid Nanofluid (2009) 7:599–619
DOI 10.1007/s10404-009-0474-x

REVIEW

Steady and unsteady flow analysis in microdiffusers and micropumps: a critical review

Majid Nabavi

Received: 6 May 2009 / Accepted: 25 June 2009 / Published online: 29 July 2009

Abstract In recent research, there has been a growing interest in the analysis of flow through microdiffusers and micropumps in order to characterize and optimize the performance of these devices. In this review, the recent advances in the numerical and experimental analysis of the steady and pulsating flows through microdiffusers and valveless micropumps are surveyed. The differences between the performance of microdiffusers and micropumps in steady and unsteady flow regimes are described. Qualitative and quantitative discussions of the effects of different design parameters on the performance of microdiffusers and valveless micropumps in both steady and unsteady flow regimes along with the contradictory results reported in the literature in this regard are provided. In addition, a summary of the latest micropump technologies along with the advantages and disadvantages of each mechanism with the emphasis on the innovative and less-reviewed micropumps are presented. Two important types of fixed microvalves, as part of valveless micropumps are described in details. Experimental flow visualization of steady and pulsating flows through microdiffusers and micropumps as a useful tool for better understanding the underlying micro-fluid dynamics is discussed. The present review reveals that there are many possible areas of research in the field of steady and unsteady flows through microdiffusers and micropumps in order to understand the effects of all important design parameters on the performance of these devices.

M. Nabavi (✉)
Department of Mechanical Engineering, McGill University, Montreal, QC, Canada
e-mail: majid.nabavi@mail.mcgill.ca

Keywords Micropumps · Microvalves · Fixed valves · Microdiffusers · Steady flow · Unsteady flow · Pulsating flow · Micro-PIV · Numerical analysis · Experimental analysis

List of symbols

u	Velocity in x direction (m/s)
v	Velocity in y direction (m/s)
$u_{\max}$	Maximum velocity in x direction (m/s)
Q	Volumetric flow rate (m^3/s)
Q_{net}	Net flow rate (m^3/s)
ρ	Density (kg/m^3)
p	Pressure (Pa)
p_0	Static pressure (Pa)
t	Time (s)
x	Axial position (m)
y	Transverse position (m)
T	Excitation period (s)
μ	Shear viscosity (kg/m s)
ν	Kinematic viscosity (m^2/s)
$Re = u_{\max} D_h/\nu$	Reynolds number
$St = \omega\, D_h/u_{\max}$	Strouhal number
$Ro = \omega\, D_h^2/\nu = Re.St$	Roshko number
$Wo = D_h/\delta$	Womersley number
V	Volume-average velocity (m/s)
P	Maximum pressure (Pa)
Δp	Frictional pressure drop (Pa)
η	Diffuser efficiency
$\eta_{\max}$	Maximum diffuser efficiency
ξ_d	Total pressure loss coefficient in the diffuser direction
ξ_n	Total pressure loss coefficient in the nozzle direction

ξ_{i-j}	Pressure loss coefficient across segment $i-j$
θ	Diffuser divergence angle (degree)
f	Excitation frequency (Hz)
ω	Angular frequency (rad/s)
D_h	Hydraulic diameter of the microdiffuser at the inlet (m)
Z	Flow impedance (kg/m^4 s)
R	Flow resistance (kg/m^4 s)
I	Flow inductance (kg/m^4)
Z_d	Flow impedance in the diffuser direction (kg/m^4 s)
R_d	Flow resistance in the diffuser direction (kg/m^4 s)
I_d	Flow inductance in the diffuser direction (kg/m^4)
Z_n	Flow impedance in the nozzle direction (kg/m^4 s)
R_n	Flow resistance in the nozzle direction (kg/m^4 s)
I_n	Flow inductance in the nozzle direction (kg/m^4)
λ	Acoustic wavelength (m)
V_{net}	Sectional net velocities (m/s)
A	Sectional area (m^2)
δ	Stokes layer thickness (m)
L	Diffuser length (m)
α	Kinetic-energy correction factor

1 Introduction

Mircoscale pumping technology has attracted a great attention in recent years. With the increasing demand of industrial and medical fields, micropumps have been applied to numerous applications (Dario et al. 2000; Woias 2005; Iverson and Garimella 2008; Amirouche et al. 2009). Some of the potential applications are drug delivery systems (LaVan et al. 2003; Junwu et al. 2005; Ma et al. 2006; Jang and Kan 2007; Hsu et al. 2007; Cui et al. 2007, 2008), lab-on-a-chip (Erickson 2005; Fair 2007; Seibel et al. 2008; Wang et al. 2008), biochemistry (Dario et al. 1996; Andersson et al. 2001; Yamaguchi and Yang 2004), controlled fuel delivery in engines (Cheng and Chien 2008) and fuel cells (Zhang and Wang 2005, 2006), localized cooling in electronics (Jiang et al. 2002; Garimella et al. 2006; Singhal, 2007; Verma et al. 2009), and micromixing (Sheen et al. 2007).

The advantage of micromachined drug delivery systems is the possibility of mass production at low cost. As a part of the drug delivery system, the micropump chip satisfies some important requirements, such as, drug compatibility, actuation safety, small size, low power consumption, and flow rate controllability over a wide range of external conditions (Teymoori and Abbaspour-Sani 2005).

Micro-fuel cells that convert the chemical energy of the fuels directly into electrical energy are considered to be the key technology for power generation in portable electronics like cellular phones and wearable electronics and have received considerable research attention in recent years. The micropump can be used to circulate fuel within a fuel cell power system (Zhang and Wang 2005, 2006).

As faster, smaller and more powerful circuit technologies are developed, heat exchange mechanisms to remove more heat become more critical. Innovative mechanisms to cool electronic components are required that use less power, run quietly, and demonstrate lasting performance in a compact size. The micropump provides a wide range of fluid handling solutions designed specifically for the needs of the electronic cooling industry (Ma et al. 2008, 2009).

To meet the demands of these cutting-edge technologies, several types of micropumps with different actuation mechanisms have been developed in recent years. Several comprehensive review papers have surveyed most of the developed microscale pumping technologies (Shoji and Esashi 1994; Laser and Santiago 2004; Woias 2005; Zhang et al. 2007; Iverson and Garimella 2008; Amirouche et al. 2009). As important part of micropumps, microvalves have been also extensively studied by many researchers (Oh and Ahn 2006; Zhang et al. 2007).

Piezoelectric micropumps with fixed microvalves are the most-investigated type of micropumps. Numerous numerical and experimental studies on the performance of this type of micropumps in steady and unsteady flow regimes can be found in the literature.

In the present review, a brief summary of the latest micropump technologies along with the advantages and disadvantages of each mechanism are provided in Sect. 2. Special emphasis is given to the innovative and less-reviewed valveless micropumps, such as, acoustic micropump, ultrasound micropumps, etc. Section 3 is devoted to a short review of different types of microvalves. In this section, the non-mechanical passive microvalves which are of great importance in designing valveless micropumps are described in details. The aim of Sects. 2 and 3 is not to duplicate the past reviews on micropumps and microvalves. The objectives of these sections are three-fold. First, to provide a brief and useful summary of the advantages and disadvantages of each mechanism which is missing in the past reviews. Second, to review and categorize the recently-developed micropumps and microvalves that have not been surveyed in the past reviews. Third, to illustrate the categorization of the piezoelectric micropumps with fixed microvalves. In Sect. 4, piezoelectric micropumps with fixed microvalves which are the most-investigated

type of micropumps are reviewed in more details, as the main objective of this study is to survey the numerical and experimental studies on the steady and pulsating flows through this type of micropumps. Sections 5 and 6 provide a critical review on the recent numerical and experimental studies on the steady and pulsating flows through different types of microdiffusers and valveless micropumps. A comprehensive perspective of the effects of different design parameters on the performance of microdiffusers and valveless micropumps in both steady and unsteady flow regimes is provided. Finally, the challenges and applications of micro-particle image velocimetry (PIV), which is the most frequently-used technique in visualizing steady and pulsating flows through microdiffusers and micropumps are discussed in Sect. 7.

2 Microscale fluid pumping: micropumps

Microscale fluid pumping mechanisms can be broadly classified into *displacement* and *dynamic* mechanisms, according to the way fluid is displaced.

2.1 Displacement micropumps

In displacement micropumps, energy is added periodically by applying a force to one or more movable pump chamber walls. Changes in chamber pressure resulting from the diaphragm motion force fluid mass through the outlet, producing a pulsating flow. Displacement micropumps can be further divided into the following sub-categories based on their actuation principle: *vibrating diaphragm* micropumps, *rotary* micropumps (Dopper et al. 1997), and *ferrofluid* micropumps (Yamahata et al. 2005a).

In the category of vibrating displacement micropumps, a pumping chamber connected to inlet and outlet valves is necessary for flow rectification. As the diaphragm deflects during the expansion mode, the pumping chamber expands resulting in a decrease in chamber pressure. When the inlet pressure is higher than the chamber pressure, the inlet valve opens and liquid fills the expanding chamber. During the compression mode, the volume of the chamber decreases with the moving diaphragm, causing the internal pressure to increase whereby liquid is discharged through the outlet valve. Various types of actuation devices have been investigated in the past decades.

Piezoelectrically actuated diaphragms (Koch et al. 1998; Park et al. 1999; Morris and Forster 2000; Fan et al. 2005; Wang et al. 2006; Hwang et al. 2007; Jang and Yu 2008; Wiederkehr et al. 2008; Hsu and Le 2008), which are among the most widely used devices for actuating micropumps, produce relatively large displacement magnitudes and forces and fast mechanical responses. A comparison of various micropump actuation mechanisms shows that piezoelectrically actuated diaphragm micropumps are among those which have high flow rates per unit area (Iverson and Garimella 2008). However, they need high input voltages (up to 400 V). *Electromagnetic actuated diaphragms* (Yamahata et al. 2005c; Lien et al. 2008) consist of a permanent magnet attached to a diaphragm and surrounded by a coil. They require a small voltage (<5 V), and have a fast response time, but they are not well compatible with microelectromechanical systems (MEMS), and require high power consumption. *Electrostatically actuated diaphragms* (Machauf et al. 2005) employ the electrostatic forces generated between electrodes to drive diaphragm. They have the advantages of fast response time, MEMS compatibility, and low power consumption, and the disadvantages of small actuator stroke and high required input voltage. *Pneumatically actuated diaphragms* (Yang et al. 2008) employ fluctuations in gas pressure on a diaphragm to produce vibration. They need low input voltages, generate high pump rates, and can be very compact, but high power consumption and long thermal time constants are their main disadvantages. *Thermally actuated diaphragms* (Yoshida 2005) use the volume expansion of a material in response to applied heat. Thermal actuation can provide large forces via large strokes, can be easily integrated with other microfluidic functionalities on a single chip, with compact footprint and low operation costs. However, they are relatively slow during the valve's closing and opening (Zhang et al. 2007). The *ionic polymer-metal composite (IPMC) actuated diaphragms* (Bennett and Leo 2004) have the ability to create a larger bending deformation under a low input voltage (2 V), and to operate not only in the liquid, but also in the air. Furthermore, the micropump manufacturing process with IPMC is convenient. However, their response as actuators is still very unpredictable. Their dynamic response is still subjected to several critical parameters that vary with time, thus extracting an accurate and repeatable prediction is very difficult (Brufau-Penella et al. 2008).

2.2 Dynamic micropumps

Dynamic micropumps involve a continuous energy source that produces a steady force on the fluid. *Electrohydrodynamic* (Ehlert et al. 2008), *magnetohydrodynamic* (Nguyen and Kassegne, 2008), *electroosmotic* (Wu et al. 2005; Lee and Li 2006; Hu et al. 2007b; Park and Lim 2008), and *electrowetting* (Mugele and Baret 2005) micropumps fall into this category. These types of dynamics micropumps have been extensively investigated and reviewed by many researchers (Iverson and Garimella 2008). However, there are some new actuation mechanisms to continuously pump fluids at microscale, which have not been reviewed in the previous reviews. These mechanisms are based on *surface*

acoustic waves (SAWs) and *acoustic streaming* (Guttenberg et al. 2004).

When a traveling SAW interacts with a liquid droplet placed on a free surface, its compressional component is diffracted at the Rayleigh angle into the droplet, generating a leaky SAW (LSAW) phenomenon caused by SAW-radiation leakage into the liquid. The LSAW component generates a pressure gradient within the droplet that results in the so-called acoustic streaming, i.e., momentum and energy transfer from the wave to the liquid. This gives rise to a liquid response that depends on the SAW power (see Fig. 1). For high-power excitation, jet propulsion or atomization can occur. At low excitation power, efficient mixing is easily obtained, whereas, at intermediate excitation powers, the entire droplet translates along the direction of the SAW propagation, producing pumping action (Renaudin et al. 2006; Cecchini et al. 2008; Du et al. 2009)

Traveling plane-wave deformations on a solid thin film immersed in a fluid can create viscous propulsion in the direction opposite to wave propagation. Tabak and Yesilyurt (2007) presented modeling and analysis of a valveless dynamic micropump that utilized a traveling plane-wave actuator. Their numerical model incorporated direct coupling between solid deforming boundaries and the fluid by means of a deforming mesh according to Arbitrary Lagrangian Eulerian implementation, and 2-D unsteady Stokes equations to solve for the flow realized by the traveling-wave actuator in the channel. Very recently, Ogawa et al. (2009) fabricated a valveless liquid pumping device by traveling waves beneath the ceiling wall induced by applying sinusoidal voltages with a phase difference of $2\pi/3$ to adjacent top electrodes (see Fig. 2). When a channel wall oscillates in the form of traveling waves, peristaltic motion is induced and the liquid beneath the wall moves along an elliptic curve. After a period of oscillation, the fluid moves slightly forward from the initial position due to fluid viscosity.

Another innovative mechanism for microfluidic transportation was reported by Hu et al. (2007a). They proposed a method by which tiny quantity of liquid could be transported in microchannels by ultrasound induced capillary action in a twisted bundle of metal wires. To make the bundle of metal wires vibrate ultrasonically, it was

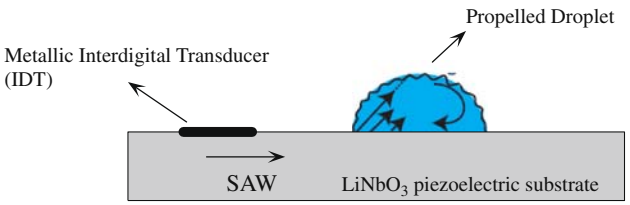

Fig. 1 Fluid translation by the use of SAWs

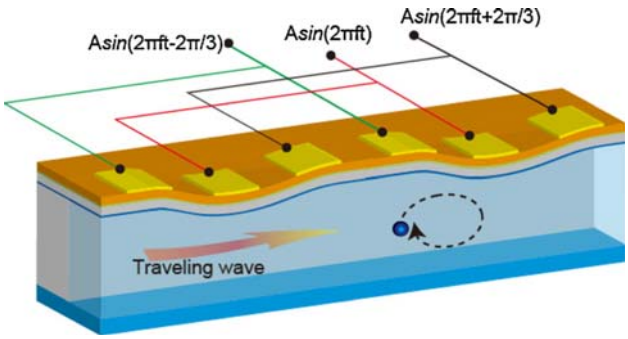

Fig. 2 A valveless micropump fabricated by Ogawa et al. (2009), which works by traveling waves beneath the ceiling wall

mechanically excited by a sandwich type ultrasonic transducer. Liquid was transported in the microchannels among the twisted metal wires. The transportation of water through the bundle of metal wires and its dependence on ultrasonic vibration were experimentally confirmed, and a physical model was proposed to explain the ultrasound induced capillary effect. The maximum capillary speed of about 15 mm/s was obtained using this method.

An optically driven micropump using viscous drag exerted on a rotating disk microrotor was developed by Maruo and Inoue (2007). The disk microrotor (diameter of 10 μm), which had three columns as targets for the optical trap, was confined to a U-shaped microchannel. To pump fluid, the disk microrotor was rotated by a time-shared optical trapping technique. The flow field inside the U-shaped microchannel was analyzed using finite element method, based on the Navier–Stokes equation. The optimized micropump was fabricated using a two-photon microfabrication technique.

Another interesting type of dynamic micropumps which combines the simplicity in design with effectiveness in pumping is the *viscous micropump*. Generally speaking, the viscous micropump consists of a cylinder asymmetrically placed inside a microchannel. When the cylinder rotates the difference in shear stresses on the lower and upper half of the cylinder creates a force imbalance that displaces the fluid. The viscous micropump was introduced by Sen et al. (1996) and has been the subject of several research papers (Sharatchandra et al. 1997; da Silva et al. 2007; Haik et al. 2007).

3 Microscale fluid rectification: microvalves

Microvalve is one of the most important components in microfluidic systems and micropumps. Microvalves can be classified into *active* microvalves, using *mechanical* and *non-mechanical* moving parts, and *passive* microvalves, using *mechanical* and *non-mechanical* moving parts (Oh and Ahn 2006).

Mechanical active microvalves employ the mechanically movable MEMS-based membranes which are coupled to magnetic (Bae et al. 2002), electric (Yang et al. 2004b), piezoelectric (Li et al. 2004), or thermal (Rich and Wise 2003) actuation methods. The actuation principles of active microvalves with non-mechanical moving parts are based on electrochemical (Suzuki and Yoneyama 2003), phase change (Pal et al. 2004), and rheological materials (Yoshida et al. 2002).

In microfluidic systems, passive microvalves play an important role. Most mechanical passive microvalves or micro-check valves are incorporated in inlets and outlets of reciprocal displacement micropumps as mechanical moving parts, such as, flaps (Paul and Terhaar 2000), membranes (Li et al. 2005), and spherical balls (Yamahata et al. 2005b). Passive valves only open to forward pressure, showing diode-like characteristics. The one way behavior of these check valves significantly affects the pumping performance of a reciprocal displacement micropump. Leakage in the check valves reduces backpressure and pumping rate in the micropump.

Non-mechanical passive microvalves, which are hereinafter referred to as *fixed microvalves*, involve no mechanical moving parts and provide the possibility to build the so-called *valveless micropumps*. Two main types of fixed microvalves have been used in valveless micropumps which are *microdiffusers* (Stemme and Stemme 1993; Gerlach et al. 1995; Olsson et al. 1999; Pan et al. 2001; Schabmueller et al. 2002; Yang et al. 2004a; Jeong and Kim 2007; Sun and Yang 2007; Hwang et al. 2008; Nabavi and Mongeau 2009) and *Tesla* microvalves (Forster et al. 2001; Feldt and Chew 2002; Morris and Forster 2003). In fixed microvalves wear and fatigue in the valves are eliminated since they have no moving parts. The risk of clogging is also reduced.

3.1 Microdiffuser

Three different microdiffuser geometries have been widely used in valveless micropumps which are, *planar* or *flat-walled* (Olsson et al. 1995, 1996a, 1999, 2000; Singhal et al. 2004; Yang et al. 2004a), *conical* (Stemme and Stemme 1993; Singhal et al. 2004), and *pyramidal* (Gerlach et al. 1995; Gerlach 1998; Olsson et al. 1996b) microdiffusers (see Fig. 3). The choice of diffuser shape is basically dependent upon the fabrication process. For planar lithography and standard micromachining fabrication techniques, planar microdiffusers are the best fit. The planar configuration widens the spectrum of possible materials and pump driver designs. Another potential advantage of the flat-walled diffuser is that, under the same inlet boundary-layer condition, the best flat-walled diffuser is 10–80% shorter than the best conical design (Olsson et al. 2000). Therefore, if space is limited in the pump design, the planar microdiffusers give the better performance.

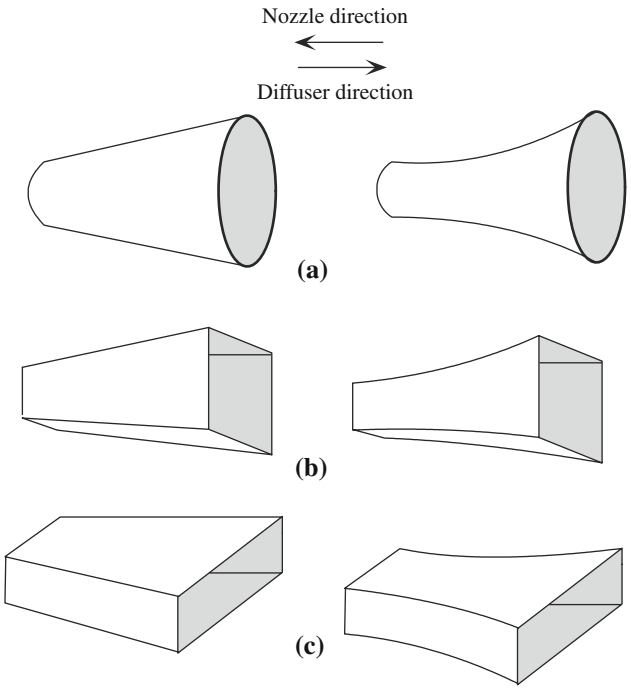

Fig. 3 Schematic of straight-wall (*left pane*) and curved-walled (*right pane*) **a** conical, **b** pyramidal, and **c** planar (*flat-walled*) microdiffusers

In order to achieve a higher rectification capability, several innovative structures for microdiffusers have been proposed, one of which is *curved-walled* microdiffuser (see Fig. 3, right pane). By the use of experimental and numerical analysis in steady flow regime, Chen et al. (2008) have shown that at a given volumetric flow rate, the pressure drop coefficient of the curved-walled microdiffuser is higher than that of the straight-wall microdiffuser.

Izzo et al. (2007) employed a new no-moving-part (NMP) microvalve in a piezoelectric micropump. The working principle of this NMP microvalve is based on the presence of vortex area inside microconduit constituting micropump valves (see Fig. 4). The use of this microvalve design allowed to achieve an enhancement of micropump performances, compared to conventional microdiffusers.

As shown in Fig. 5, a microdiffuser is composed of three segments, entrance (segment 1–2), diffuser (segment 2–3), and exit (segment 3–4) segments (Wang et al. 2009). The frictional pressure loss across segment i–j is defined as

$$\Delta p_{i-j} = p_i - p_j + \frac{1}{2}\alpha_i \rho V_i^2 - \frac{1}{2}\alpha_j \rho V_j^2, \quad (1)$$

where $\alpha = \frac{1}{V^3 A}\int u^3 \mathrm{d}A$ is kinetic-energy correction factor.

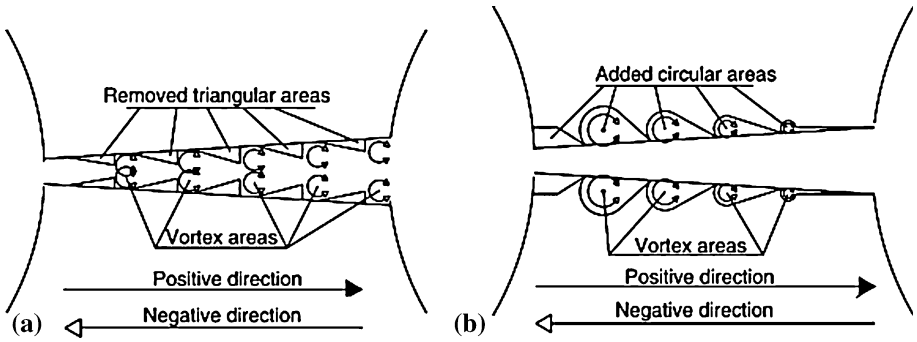

Fig. 4 Schematic location of vortex areas in **a** the series-NMP (S-NMP) microvalve and in **b** the recirculation-NMP (R-NMP) microvalve. The *empty arrows* show the flowing path in the negative direction whereas the *full arrows* show the flowing path in the positive one (Izzo et al. 2007)

The pressure loss coefficient across segment $i-j$ is then defined as

$$\xi_{i-j} = \frac{\Delta p_{i-j}}{\frac{1}{2}\rho[\max(V_i^2, V_j^2)]}. \tag{2}$$

By the use of Eqs. 1 and 2 and the continuity equation ($V_iA_i = V_jA_j$), the total pressure loss coefficients of the microdiffuser shown in Fig. 5 across the diffuser direction (ξ_d) and the nozzle (ξ_n) are defined as,

$$\begin{aligned}\xi_d &= \frac{\Delta p_{1-4}}{\frac{1}{2}\rho V_2^2} = \xi_{1-2} + \xi_{2-3} + \xi_{3-4}\left(\frac{A_2}{A_3}\right)^2,\\ \xi_n &= \frac{\Delta p_{4-1}}{\frac{1}{2}\rho V_2^2} = \xi_{4-3}\left(\frac{A_2}{A_3}\right)^2 + \xi_{3-2} + \xi_{2-1},\end{aligned} \tag{3}$$

where,

$$\begin{aligned}\xi_{1-2} &= \frac{p_1 - p_2}{\frac{1}{2}\rho V_2^2} + \alpha_{d,1}\left(\frac{A_2}{A_1}\right)^2 - \alpha_{d,2},\\ \xi_{2-3} &= \frac{p_2 - p_3}{\frac{1}{2}\rho V_2^2} + \alpha_{d,2} - \alpha_{d,3}\left(\frac{A_2}{A_3}\right)^2,\\ \xi_{3-4} &= \frac{p_3 - p_4}{\frac{1}{2}\rho V_3^2} + \alpha_{d,3} - \alpha_{d,4}\left(\frac{A_3}{A_4}\right)^2,\\ \xi_{4-3} &= \frac{p_4 - p_3}{\frac{1}{2}\rho V_3^2} + \alpha_{n,4}\left(\frac{A_3}{A_4}\right)^2 - \alpha_{n,3},\\ \xi_{3-2} &= \frac{p_3 - p_2}{\frac{1}{2}\rho V_2^2} + \alpha_{n,3}\left(\frac{A_2}{A_3}\right)^2 - \alpha_{n,2},\\ \xi_{2-1} &= \frac{p_2 - p_1}{\frac{1}{2}\rho V_2^2} + \alpha_{n,2} - \alpha_{n,1}\left(\frac{A_2}{A_1}\right)^2.\end{aligned} \tag{4}$$

Combining Eqs. 3 and 4 results in,

$$\begin{aligned}\xi_d &= \frac{p_1 - p_4}{\frac{1}{2}\rho V_2^2} + \alpha_{d,1}\left(\frac{A_2}{A_1}\right)^2 - \alpha_{d,4}\left(\frac{A_2}{A_4}\right)^2,\\ \xi_n &= \frac{p_4 - p_1}{\frac{1}{2}\rho V_2^2} + \alpha_{n,4}\left(\frac{A_2}{A_4}\right)^2 - \alpha_{n,1}\left(\frac{A_2}{A_1}\right)^2.\end{aligned} \tag{5}$$

The total loss of the microdiffuser has three components, the entrance loss, the diffuser loss, and the exit loss. Wang et al. (2009) discussed the entrance loss strongly depends on the entrance geometry and Reynolds number ($Re = u_{max}D_h/\nu$). Whereas, the exit loss is strongly influenced by the diverging angle due to the highly non-uniform velocity profile downstream of the diffuser. Considerable entrance loss exists even for a well rounded entrance. They also found that the common assumption of unity exit loss used in the literature on valveless micropumps can cause significant error.

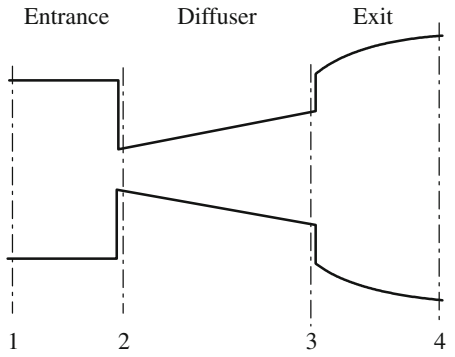

Fig. 5 Schematic of microdiffuser segments

The resulting microdiffuser efficiency ratio is then calculated as

$$\eta = \frac{\xi_n}{\xi_d}. \tag{6}$$

If $\eta > 1$, a pumping action from the inlet to the outlet is achieved. The higher the η, the higher the flow-directing efficiency and net flow rate through the microdiffuser.

3.2 Tesla microvalve

There are a variety of NMP valve designs. Forster et al. (1995) presented techniques for design and testing of fixed microvalves including the Tesla-type and the diffuser valve. The simplest configuration is shown in Fig. 6, which is roughly similar to that designed in the macro-scale by Tesla (1920). It has a bifurcated channel that re-enters the main flow channel perpendicularly when the flow is in the reverse direction. In the forward direction, the majority of the flow is carried by the main channel with reduced

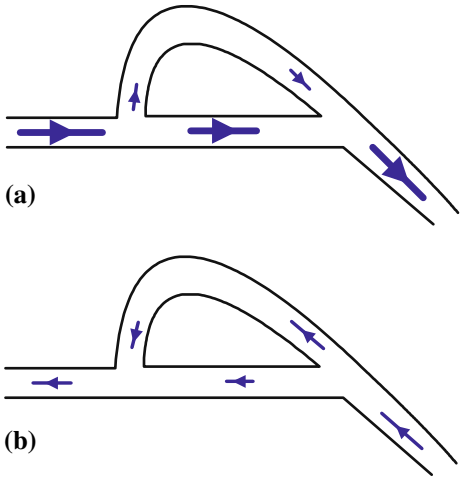

Fig. 6 Tesla microvalve; **a** In the forward direction, the majority of the flow is carried by the main channel with reduced pressure losses, **b** in the reverse direction, a bifurcated channel re-enters the main flow channel perpendicularly

pressure losses. In a numerical study, Deshpande et al. (1998) analyzed both Tesla and diffuser microvalves. Based on their study, Tesla microvalves are expected to provide higher rectification capability than diffuser microvalves. Morris and Forster (2003) developed a model for Tesla-valve micropumps based on first principles, with no experimental or otherwise empirical information needed to predict resonant behavior. Their model made possible the determination of optimal valve size.

4 Piezoelectric micropumps with fixed microvalves

Piezoelectric micropumps with fixed microvalves (*reciprocating valveless micropumps*) are the most-investigated type of vibrating displacement micropumps. In order to characterize and optimize the performance of this type of micropumps, several numerical and experimental studies have been performed. By the use of these studies, better understanding of the physics of microscale pumping action as well as microfluid dynamics of the steady and unsteady flows in microdiffusers and micropumps has been gained.

Piezoelectric micropumps with fixed microvalves involve the oscillation of a diaphragm excited by a piezoelectric actuator, propelling the flow through two passive fixed microvalves which direct the flow. The idea of using microdiffuser was first presented by Stemme and Stemme (1993). Gerlach et al. (1995) extended this idea to microscale and presented the working principle of a reciprocating micropump and discussed its basic parameters. The proposed valveless diffuser micropump consists of two diffuser elements connected to a micropump chamber with an oscillating diaphragm as shown in Fig. 7a. The oscillating diaphragm forces the fluid through the two diffuser elements. The result is a net transport of fluid from the inlet to the outlet due to the difference in the flow resistances in the forward (diffuser) and reverse (nozzle) directions. The operation of this pump can be divided into the suction mode and discharge mode. During the suction mode, the diaphragm is moving upwards to increase the fluid volume inside the chamber. The flow rate through the inlet is greater than the flow rate through the outlet. In this mode, the inlet microdiffuser acts as diffuser while the outlet microdiffuser acts as a nozzle. In the discharge mode, the membrane is moving downwards to reduce the volume inside the chamber. In this mode, the outlet element performs as a diffuser and the inlet element acts as a nozzle. Therefore, the flow rate through the outlet is greater than the flow rate through the inlet. The operation of these two modes forms a complete pumping cycle to transfer the fluid from the inlet reservoir to the outlet reservoir. The inlet and outlet microdiffusers can be placed in parallel with the diaphragm as shown in Fig. 7b. Flow rectification can be also accomplished in Tesla microvalves by inducing larger pressure losses in the reverse direction compared to those in the forward direction, assuming the same flow-rates, as shown in Fig. 7c.

Very recently, a new diffuser-based pumping mechanism has been proposed by the author and his co-workers, which is able to pump fluids at both macroscale (*valveless standing wave pump*) (Nabavi et al. 2008a) and microscale (*valveless acoustic micropump*) (Nabavi and Mongeau 2009). In reciprocating valveless micropumps, a moving diaphragm does pressure work on the working fluid in a periodic manner. However, in the valveless acoustic micropump, pressure fluctuations are achieved through the establishment of linear or nonlinear standing waves (Nabavi et al. 2007a, 2008b) inside the micropump chamber (see Fig. 8a). Assuming a linear standing wave inside the chamber, the pressure is assumed to be nearly sinusoidal, with a maximum amplitude of P and an angular frequency of ω, $p(t) = P\sin(\omega t)$ at the outlet port (pressure anti-node), and atmospheric at the inlet port (pressure node). When $p(t) > 0$ (the discharge mode, Fig. 8b) the microdiffuser acts as a diffuser and for $p(t) < 0$ (the suction mode, Fig. 8c) the microdiffuser operates like a nozzle. For equal pressure fluctuation amplitudes in the pump and suction modes, the volume of the outgoing flow through the outlet port is larger than the incoming flow, due to the lower flow resistance in the diffuser direction than that in the nozzle direction. Therefore, a net mass flow rate can be achieved.

5 Steady flow analysis through fixed microvalves

The velocity fields in piezoelectric micropumps with fixed microvalves are pulsatile and the unsteadiness of the flow

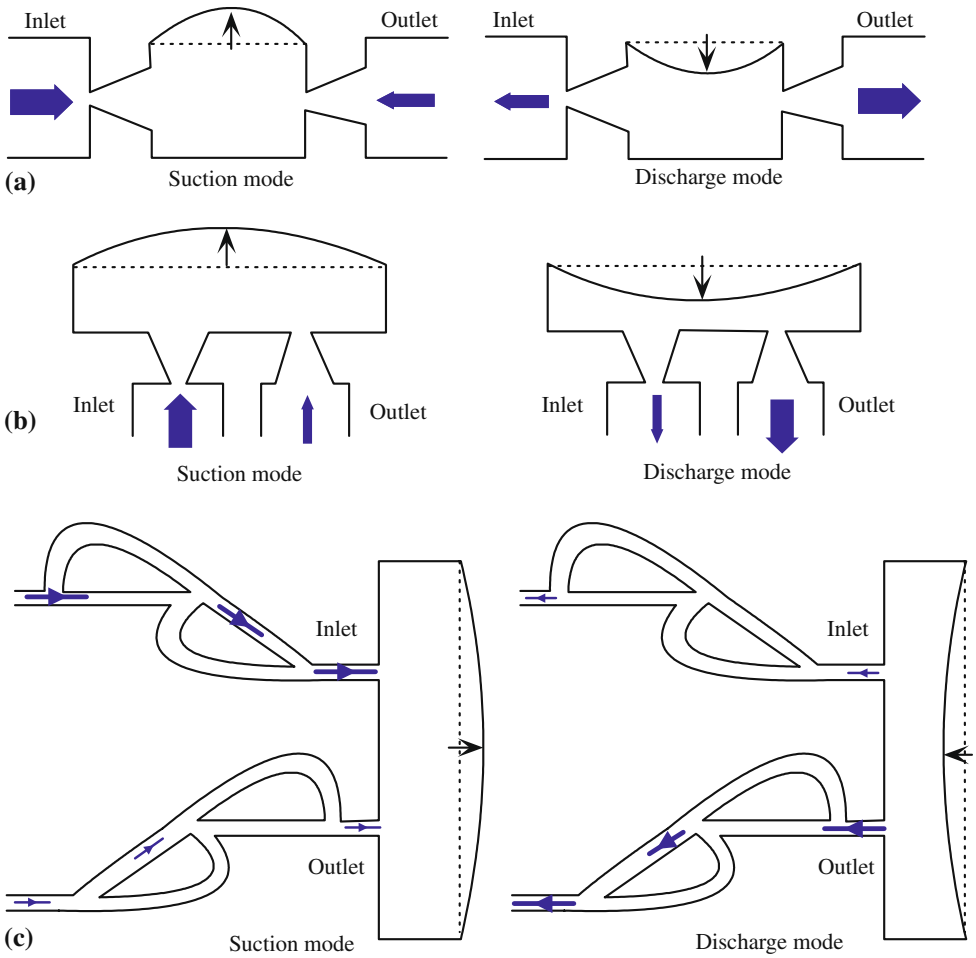

Fig. 7 Reciprocating valveless micropumps by the use of **a** microdiffuser in parallel-geometry, **b** a microdiffuser in perpendicular-geometry, and **c** Tesla microvalve

affects the performance of the microdiffusers. However, the efficiency of a microdiffuser is almost frequency independent at low frequencies (small Roshko numbers, $Ro = \omega D_h^2/\nu = R_e \cdot St$) (Sun and Huang, 2006; Ahmadian et al. 2006). Therefore, steady flow analysis of microdiffusers may be used for the design of diffuser micropumps at low frequencies.

Studies on frictional pressure drop and laminar to turbulent transition in microchannels in steady flow regime have reported some inconsistent and contradictory results. Mala and Li (1999) reported that the friction factor in microchannels is higher than that predicted by the conventional theory. They attributed this to an early transition from laminar to turbulent flow. Peng et al. (1994) gave $Re = u_{max} D_h/\nu < 400$ for laminar flow, $400 < Re < 1{,}000$ for the transition region and $Re > 1{,}000$ for fully turbulent flow. Hsieh et al. (2004) argued that pressure drops bigger than those predicted by the conventional theory would occur in microchannels. The onset of transition was found at $Re \simeq 240$. However, the authors of the more recent study (Kohl et al. 2005) supported the standard findings that laminar flow is maintained for $Re < 2{,}300$, and that friction factors for microchannels can be accurately determined from data for standard large channels. They attributed the large inconsistencies in previously published data to instrumentation errors and/or improper accounting for compressibility effects.

The microdiffuser plays an important role in the performance of reciprocating micropumps. Steady flow through different types of microdiffusers has been extensively investigated both numerically and experimentally. Some of these studies are summarized in Table 1. In this Table, area ratio is defined as the ratio of the outlet area to the inlet area, and slenderness is defined as the ratio of the diffuser length to the inlet width. All studies were performed with water as the working fluid, except Chen et al. (2008) in which air was used. Olsson et al. (1996b) performed their experiments in both water and methanol to investigate the effect of fluid type on the performance of microdiffusers.

Stemme and Stemme (1993) designed and tested the first diffuser-based micropump based on the flow rectification property of diffusers, and made measurement on single diffuser/nozzle element for stationary water flow in order to understand its working characteristics. They found that

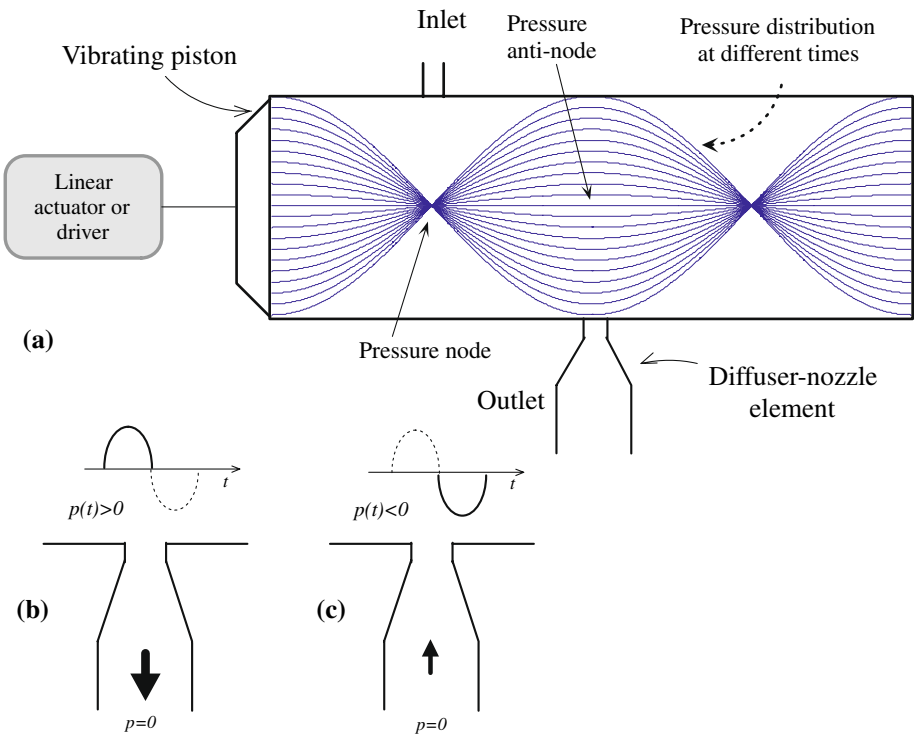

Fig. 8 Flow rectification process in valveless acoustic micropump, **a** pump mode, and **b** suction mode

the loss coefficient of the nozzle, ξ_n, was always larger than the loss coefficient of the diffuser, ξ_d, for the same pressure drop. It means that the diffuser efficiency, η, was always larger than unity in the investigated pressure-drop interval. Moreover, η, ξ_d, and ξ_n, were approximately constant throughout the investigated turbulent ($Re > 2{,}300$) flow regime, whereas, ξ_n and ξ_d decreased, and η increased as Re was increased in the laminar flow regime ($Re < 2{,}300$). The efficiency ratio was also constant for very low flow velocities where ξ_n and ξ_d were very high.

Olsson et al. (1996b) performed stationary flow measurements on five different single pyramidal microdiffusers. They found that the small-angle diffuser had lower diffuser efficiency than the diffusers with larger diffuser angles, and that the diffuser length had no significant impact on the diffuser efficiency. Water and methanol were used as the working fluids and diffuser efficiency was found to be greater for methanol than for water. This was attributed to turbulent flow in methanol for Reynolds numbers in the range of 140–180 as opposed to laminar flow in water for Reynolds numbers of 100–120.

Jiang et al. (1998) analyzed the microdiffuser flow with different Reynolds numbers and conical angles experimentally. They found that the nozzle pressure coefficient was always bigger than the diffuser pressure coefficient at the experiment Reynolds number range (<2,000), and both ξ_n and ξ_d decreased with increasing pressure drop or Re. For the same microdiffuser, η remained constant within the experiment Re. Their experimental results of microdiffuser with angles of 5°, 7.5°, and 10° demonstrated that, at the experiment Re range, ξ_n, ξ_d, and η decreased with an increase in θ from 5° to 10°.

Olsson et al. (2000) performed an investigation of flat-walled diffuser elements for valveless micropumps. Their measurements showed that the better flow directing capability was obtained with the smaller opening angle. They found that the longer element showed the best flow-directing capability, while the pump performance measurements of the shorter element was the best. They argued that this difference could be due to differences in the flow behavior for static and dynamic diffuser flow. No significant difference in the flow-pressure characteristics between turbulent and laminar simulations was seen. They also found that η decreased with increasing Re and with increasing θ from 7° to 13°.

Singhal et al. (2004) analyzed the steady flow through microdiffusers using the commercially available software Fluent. They observed that flow rectification through the microdiffuser was possible for very low Reynolds number laminar flows. The variation of ξ_d with Re followed opposite trends for small and large diffuser angles. For $\theta < \theta_{cr}$, an increase in Re resulted in decreasing ξ_d, while for $\theta > \theta_{cr}$, an increase in Re caused an increase in ξ_d. The values of θ_{cr} for conical and planar microdiffusers were about 10° and 20°, respectively. For both conical and planar microdiffusers, the curves of ξ_d versus diffuser angle had

Table 1 Recent studies on steady flow through different types of microdiffusers

Study	Diffuser type/ entrance and exit losses	Diffuser angles	Area ratio	Slenderness	Range of *Re*	Main results
Stemme and Stemme (1993) experimental	Conical/ included	5.3°, 10.7°	2.1, 2.6	5.7, 17.4	<10,000	$\xi_n > \xi_d$ for both laminar and turbulent *Re* ξ_n and ξ_d decrease, and η increases as *Re* increases for $Re < 2{,}300$ ξ_n, ξ_d and η are almost constant for $Re > 2{,}300$
Olsson et al. (1996b) experimental	Pyramidal/ included	1.9°–6.8°	1.8–5.4	14–37	<170	η is higher for methanol than that for water η slightly increases with increasing *Re* η increases with an increase in θ from 1.9° to 6.8°
Jiang et al. (1998) experimental	Conical/ included	5°, 7.5°, 10°	12.9, 18.4, 23.8	60	<2,000	ξ_n, ξ_d and η decrease with an increase in θ from 5° to 10° ξ_n and ξ_d decrease with an increase in *Re* η is almost constant with increasing *Re*
Olsson et al. (2000) numerical and experimental	Planar/ included	7°, 9.8°, 13°	2.7, 3.4, 4.1	13.7, 18	<1,350	η decreases with increasing *Re* η decreases with increasing θ from 7° to 13° No significant difference in the flow-pressure characteristics between turbulent and laminar simulations was seen
Singhal et al. (2004) numerical	Planar and conical/not included	5°–140°	–	–	200, 500, 1,000	Curve of ξ_d versus *Re* follows opposite trends for small and large θ Curves of ξ_d versus θ have minimum at $10° < \theta < 20°$, depends on *Re* As θ increases, flow separation occurs
Yang et al. (2004a) experimental	Planar/ included	10°, 40°	2.8, 8.3	10	50–400	ξ_d, ξ_n, and η decrease with increasing *Re* ξ_d and ξ_n decrease with increasing θ At a given *Re*, ξ_n is always greater than ξ_d The influence of the diffuser length on the ξ is small Curves of ξ_d and ξ_n versus diffuser depth have a minimum η decreases with increasing *Re*
Sun and Yang (2007) experimental	Planar/ included	10°–110°	8–58	20	<22	η_{max} was accomplished at $\theta = 60°$ ξ_n is always larger than ξ_d For $\theta \leq 40°$, there is no flow separation in microdiffuser For larger *Re*, flow separation starts at smaller θ ξ_d and ξ_n decrease with increasing θ η decreases with increasing *Re*
Chen et al. (2008) experimental	Planar/ included	10°, 20°	2.75, 4.53	10	<80	ξ_d and ξ_n decrease with increasing *Re* or θ At a given *Re*, the values of ξ_d and ξ_n of the curved structure are larger than those of the straight structure with the same width of inlet/outlet The overall diffuser efficiency of two structures are almost the same
Wang et al. (2009) numerical and experimental	Planar/ included	4°–120°	1.3–53	15	100–2,000	ξ_d, ξ_n, and η decrease with increasing *Re* η_{max} is found at $\theta = 40°$ for $Re = 100$, and at $\theta = 20°$ for $Re \geq 500$ η is greater than unity, except for $\theta \geq 120$ and $Re \geq 2{,}000$ For $\theta \leq 10°$ no flow separation occurs, for $\theta \geq 20°$ flow separation occurs and starts from the frontal surface

minimum at $10° < \theta < 50°$, depending on *Re*. Hence, the Reynolds number of the flow should be considered in the design of micropumps employing such valves. As the diffuser angle was increased, flow separation occurred, which was associated with higher loss coefficients (higher than the viscous contributions). Since flow separation was more dominant for higher *Re*, loss coefficients at the larger cone angles were also greater for larger *Re*.

Experimental investigations of the performance of microdiffuser were performed by Yang et al. (2004a). They found

that the pressure loss coefficients of the nozzle and diffuser decreased as the Reynolds number was increased. At a given Reynolds number, the pressure loss coefficient of the nozzle was higher than that of the diffuser due to a considerable difference in momentum change. At a fixed Reynolds number, the pressure loss coefficients for the element with a larger angle were smaller than those for the element with a smaller angle. The influence of the microdiffuser length on the pressure loss coefficient was found to be small. At a fixed volumetric flow rate, a minimum of the pressure loss coefficient versus microdiffuser depth was observed.

Sun and Yang (2007) investigated the effects of the diffuser angle on the flow rectification of a microdiffuser in the steady flow regime for $Re \leq 22$. Their results showed that the flow rate in the diffuser direction was always larger than that in the nozzle direction for $10° \leq \theta \leq 110°$, regardless of the diffuser angle. For their testing conditions (steady, $Re \leq 22$), the best flow rectification was accomplished at $\theta = 60°$. They argued that the occurrence of the flow separation plays an important role in the flow rectification performance of microdiffusers. For $\theta \leq 40°$, the flow was attached and the flow rates in both diffuser and nozzle directions increased as θ was increased. For $\theta > 40°$, flow separation occurred in the diffuser direction. The vortex pair suppressed the core flow and resulted in poor flow rectification. Hence, the volume flow rate in the diffuser direction was nearly independent of the angle for $\theta > 40°$. In the nozzle direction, however, the flow remained attached and the corresponding flow rate slightly increased with θ. This increase of the flow rate in the nozzle direction was assumed to be a key factor for poorer flow rectification in microdiffuser with a larger angle.

Chen et al. (2008) presented the results of a study on the fabrication and testing of curved-walled microdiffusers with air as the working fluid. They found that the pressure loss coefficients of the curved-walled microdiffuser structure decreased with the opening angle, and the pressure loss coefficients varied slightly when $Re > 60$. At a given Reynolds number, the values of ξ_d and ξ_n of the curved structure were larger than those of the straight structure with the same width of inlet/outlet. However, the overall diffuser efficiency of two structures was almost the same.

Wang et al. (2009) investigated the loss characteristics and flow rectification performance of flat-walled microdiffusers ($4° \leq \theta \leq 120°$) at steady flow regime for $100 \leq Re \leq 2{,}000$ which was considered deficient in the literature. They found that the flow separation plays a significant role in reducing diffuser loss. Based on their experimental and computational results, for small diverging angles, no separation occurred. As the diverging angle increased until flow separation occurred from the frontal surface and formed a large circulation zone, the total loss of the diffuser dropped down to a minimum due to a considerable reduction of wall shear stresses and became less sensitive to the diverging angle and Reynolds number thereafter. The diffuser angle for optimum diffuser efficiency was found to decrease from 40° at $Re = 100°$ to 20° for $Re > 500$. The total pressure loss coefficient of the microdiffuser decreased with increasing Reynolds number. For a fixed Reynolds number, the total loss in the diffuser was smaller than that in the nozzle except for the diffuser with a very large diverging angle ($\theta \geq 120°$) and $Re \geq 1{,}000$.

5.1 Effects of different design parameters

Review of the above-mentioned studies reveals that different design parameters, such as, diffuser shape and angle, fluid properties, and Reynolds number have great impacts on the performance of microdiffusers and valveless micropumps in the steady flow regime. A summary of these effects is provided in the following:

1. Effects of Reynolds number:
   - Both ξ_n and ξ_d decrease with increasing Re, regardless the type of microdiffuser (planar, conical, or pyramidal), the diffuser angle, and the working fluid (Stemme and Stemme 1993; Jiang et al. 1998; Olsson et al. 2000; Yang et al. 2004a; Chen et al. 2008; Wang et al. 2009). However, Singhal et al. (2004) reported an increase in ξ_d with an increase in Re at $\theta > 20°$ for planar and conical microdiffusers.
   - For a planar microdiffuser, η decreases with increasing Re, regardless the diffuser angle (Olsson et al. 2000; Yang et al. 2004a; Wang et al. 2009).
   - For a conical microdiffuser, η is almost independent of Re in turbulent flow regime (Stemme and Stemme 1993). In laminar flow regime, for small diffuser angle ($\theta < 10°$), Stemme and Stemme (1993) and Singhal et al. (2004) reported increasing η, with increasing Re, whereas, Jiang et al. (1998) reported that η was almost independent of Re. In laminar flow regime, for large diffuser angle ($\theta > 20°$), Singhal et al. (2004) reported a slight decrease in η, with increasing Re.
   - For a pyramidal microdiffuser, η increases with increasing Re (Olsson et al. 1996b).
2. Effects of diffuser angle:
   - For all types of microdiffusers, both ξ_n and ξ_d decrease with increasing θ, regardless the Reynolds number and working fluid. (Olsson et al. 1996b; Jiang et al. 1998; Yang et al. 2004a; Sun and Yang, 2007; Chen et al. 2008; Wang et al. 2009). However, according to Singhal et al. (2004), for both planar and conical diffusers, ξ_d decreases with

an increase in θ at $\theta < 20°$, and then increases with an increase in θ at $\theta > 20°$.

- For a planar microdiffuser, Olsson et al. (2000) reported that η decreased with increasing θ from 7° to 13° at $Re < 1{,}350$. However, Sun and Yang (2007) and Wang et al. (2009) found that η increased with increasing θ up to a critical value of diffuser angle (θ_{cr}), and decreased with further increase of θ beyond θ_{cr}. Wang et al. (2009) found that the diffuser angle for optimum diffuser efficiency decreased from 40° at $Re = 100$ to 20° for $Re > 500$. θ_{cr} was found to be 60° for $Re < 22$ by Sun and Yang (2007).
- For a conical microdiffuser, η decreases with an increase in θ (Jiang et al. 1998; Singhal et al. 2004).
- For a pyramidal microdiffuser, η increases with an increase in θ from 1.9° to 6.8° (Olsson et al. 1996b).

3. Effects of working fluid:

- Efficiency of the microdiffuser is higher for a liquid with lower viscosity (methanol) than that for a liquid with higher viscosity (water) (Olsson et al. 1996a, b).

4. Flow separation:

- Flow separation plays a significant role in reducing diffuser loss (Wang et al. 2008).
- According to Wang et al. (2008), for a small θ, there is no flow separation in the diffuser. As θ increases to 20°, separation occurs at a location about one-third of the diffuser length and forms a large circulation zone on the wall. At the same time, the loss coefficient drops down to a minimum. Further increase in the diverging angle leads to a forward movement of the separation point and slightly increase in ξ_d. For $\theta \geq 80°$, separation starts immediately after the entrance and ξ_d remains almost constant thereafter.
- Based on the study of Sun and Yang (2007), for $\theta < 30°$, there is no flow separation in the planar microdiffuser and the flow attaches to the sidewalls. As θ increases to 30°, a small pair of recirculation regions is observed near the throat. For $\theta > 40°$, the flow always separates and two symmetric recirculation regions are seen. When the driving pressure increases, the separation point moves upstream while the reattachment point moves downstream, resulting in larger separation vortices.

Figure 9 shows the typical shape of flow field inside the planar microdiffuser of different angles in steady flow regime. The figure clearly shows that for small values of θ, there is no flow separation in the planar microdiffuser. As θ increases beyond a critical value, separation occurs.

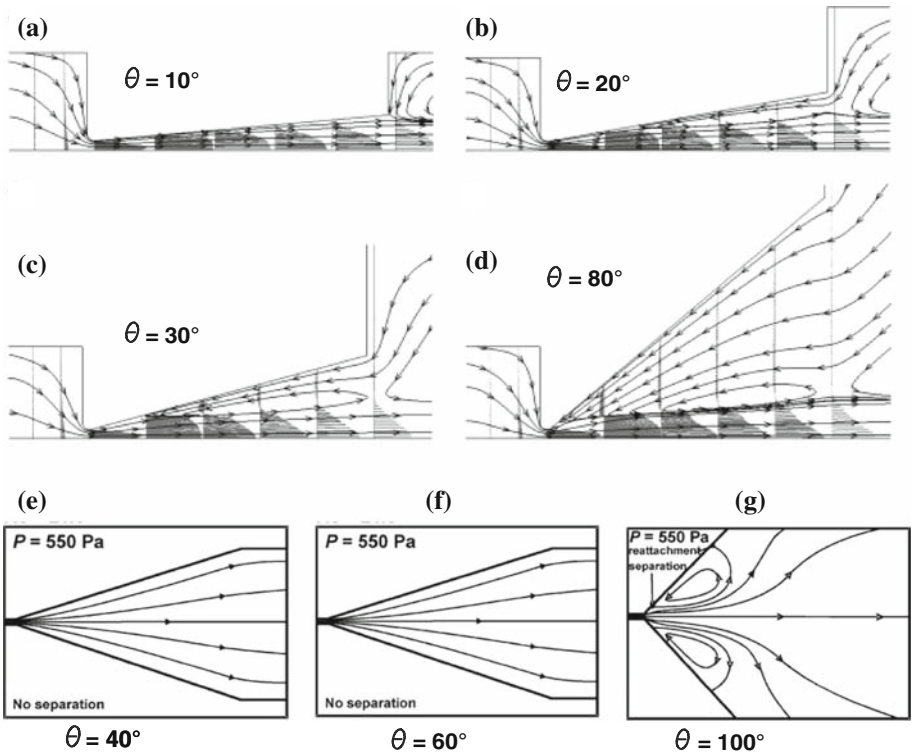

Fig. 9 Flow field inside the planar microdiffuser in steady flow regime from Wang et al. (2009) and Sun and Yang (2007)

6 Unsteady flow analysis through fixed microvalves

Several nonlinear and complicated phenomena are happening in the unsteady flow regime through microdiffusers, which have significant effects on the performance of microdiffusers and valveless micropumps. The phase difference between pressure and velocity waveforms, and the large scale flow recirculation regions inside the microdiffuser are among these phenomena.

In unsteady flow regime, the Womersley number, $Wo = D_h/\delta$, is used to describe the unsteady nature of fluid flow in response to an unsteady pressure gradient ($\delta = \sqrt{2\nu/\omega}$ is the Stokes layer thickness). Small values of Wo (1 or less) indicate that viscous effects are dominant and that the frequency of pulsation is sufficiently low so that a parabolic velocity profile has time to develop during each cycle, and the flow is nearly in phase with the pressure gradient. In this regime, the microdiffuser performance is frequency-independent. Large values of Wo (20 or more) implies that the frequency of pulsation is sufficiently large so that the velocity profile is relatively flat, and the mean flow lags the pressure gradient by about $\pi/2$. For $Wo > 1$, the microdiffuser performance is frequency-dependent.

Several experimental and numerical studies on unsteady flow through different types of microdiffusers have been reported in the literature which are summarized in Table 2. These studies were performed with water as the working fluid. In Sun and Huang (2006), Wang et al. (2007) and Nabavi and Mongeau (2009) single microdiffuser has been investigated, whereas, the total pump has been analyzed in the rest of the studies.

Pan et al. (2001) suggested an optimal frequency range for reciprocating valveless micropumps based on an analytical model. They found that the ratio of the pressure loss coefficients of diffuser and the coupling parameter plays an important role. Generally, the lower this ratio is, the higher will be the mean flux. Also, for a valveless membrane micropump, there exists an optimal working frequency range. Usually, this optimal working frequency region is around 0.1 times the first natural frequency of the membrane.

Sun and Huang (2006) performed a numerical study of the unsteady flow through a microdiffuser by the use of the commercially available software Fluent. They examined the effects of two primary parameters, diffuser angle ($\theta = 10°$–$110°$.) and excitation frequency ($f = 1$–$1{,}000$ Hz) on the diffuser performance. They found that microdiffusers with larger diffuser angles feature better rectification capability for $10° \leq \theta \leq 70°$. The net flow rate obtained was nearly independent of θ for $\theta > 70°$. Their computational results also yielded that the net flow rate was independent of excitation frequency for $f < 25$ Hz, but decreased with increasing frequency for $f > 25$ Hz. Hence, the role of excitation frequency was classified into three different regimes by the Roshko number ($Ro = \omega D_h^2/\nu$), frequency independent regime ($Ro < 0.25$), transition regime ($0.25 < Ro < 2$) and frequency dependent regime ($Ro > 2$). They also found that with the dynamic actuation mechanism, flow separation was inevitable for microdiffuser regardless of its angle, excitation frequency and corresponding Reynolds number. The size and life time of flow separation increased with increasing θ.

Ahmadian et al. (2006) obtained the fluid flow response to actuation frequency of a microdiffuser under harmonic pressures by the use of a 2-D model of a micropump valves and chamber. Their analysis was performed for 10 kPa back pressure on micropump chamber and actuation frequencies within the range of 1–10 kHz. Their results showed that for low frequencies, a parabolic velocity profile was observed at the valve midway, while, instabilities with the tendency of transition to boundary layer dominant profile was observed for high actuation frequencies. Oscillating flow in diffuser indicated existence of high shear stress regions near the wall along with the flow reversal in the center at high frequencies. Both valve and pump net flow rate decreased drastically as the frequency approached a certain value. Flow rate was approximately in phase with actuation at low frequencies but phase shift ascended as actuation frequency was increased. The main head loss of flow occurred at the diffuser valves while sudden contraction and expansion of streamlines at the diffuser entrance and exit involved only 22% of the total energy.

Wang et al. (2007) investigated the performances of microdiffusers under both steady and unsteady flow conditions. They concluded that Reynolds number confirmed by steady analysis should be greater than 10 to be more effective. An optimal Strouhal number ($St = \omega D_h/u_{max}$) with maximum net volume flow rate was found at $St = 0.013$ for the unsteady flow condition. Net flow rate per period was independent of St for $St < 0.001$, and decreased with increasing St for $St > 0.001$. The flow field was basically oscillating with a non-zero mean because of its asymmetry and the net mass flow would appear naturally. They concluded that the driving frequency and the net volume flow are the two most important parameters in studying the efficiency of the valveless reciprocating micropumps.

Yao et al. (2007) performed 3-D transient and full structure/fluid coupling CFD simulation of flows in a PZT micropump with pyramidal microdiffuser at different frequencies of 8, 50, 100, 200, and 500 Hz. They found that net flow rate increased rapidly with increasing frequency, and reached the peak at $f = 250$ Hz, then decreased slowly with further increase in frequency.

Table 2 Recent studies on unsteady flow through different types of microdiffusers

Study	Diffuser type/ Entrance and exit losses	Diffuser angles	Area ratio	Slenderness	Range of f (Hz)	Range of Re	Range of Wo	Main results
Sun and Huang (2006) numerical	Planar/not included	10°–110°	4–58	10	1–1,000	<63	0.16–5.2	η increases with increasing θ from 10° to 70° The flow rate is nearly independent of θ, for $\theta > 70°$ The flow rate is independent of f for $f < 25$ Hz, but decreases with increasing f for $f > 25$ Hz The size and life time of flow separation increase with an increase in θ
Ahmadian et al. (2006) numerical	Planar/ included	8°	2.4	20	1–10,000	100–500	0.18–17.7	Both valve and pump net flow rate decrease as f approaches a certain value (100 Hz) Q and p are in phase at low frequencies, but phase shift ascends as f is increased The main head loss occurs at the diffuser segment Entrance and exit losses are only 22% of the total energy loss
Wang et al. (2007) numerical and experimental	Planar/ included	40°, 120°	2–3.33	–		30–320	–	The maximum net flow rate is found at $St = 0.013$ Linear relation between the driving pressure amplitude and net volume flow rate is observed Net flow rate increases as Re increases
Yao et al. (2007) Numerical	Pyramidal/ included	6°	7.5	31.25	8–500	<200	2–15.8	Q increases rapidly with increasing f Q_{max} occurs at $f = 250$ Hz Q decreases slowly with further increasing f
Tanaka et al. (2008) experimental	Planar/not included	10°–90°	5	2–22.7	20–140	<1,700	3–21	Maximum flow rate is achieved at $\theta = 50°$ Flow rate increases with increasing Re Flow rate increases with increasing f
Sheen et al. (2008) experimental	Planar/ included	7°	3.37	27.5	1,000–3,000	<115	2.24–3.88	The maximum flow rate occurs at $f = 1.9$ kHz The volume flow increases linearly with V_{pp}
Tsui and Lu (2008) numerical	Planar/ included	7°	2.22	20	2,200	–	8.3	ξ decreases as back pressure increases
Hwang et al (2008) Numerical and experimental	Planar/ included	6°	1.84	–	50–4,000	Laminar	2.38–6.72	The maximum flow rate is achieved at $f = 225$ Hz Higher flow rate is achieved with increasing V_{pp} Maximum flow rate is obtained for a 4.5 mm chamber radius
Nabavi and Mongeau (2009) numerical	Planar/not included	30°–120°	6.36–35.6	10	10,000–30,000	<50	46–80	Net flow rate and η increase with an increase in Re or a decrease in f η increases with increasing θ from 30° to 90° The flow rate is nearly independent of θ, for $\theta > 90°$ The life time and size of the flow circulation for the high frequency cases are smaller than those for the low frequency cases The phase difference between pressure and velocity at high frequency is almost $\pi/2$, whereas this value at low frequencies is significantly less than $\pi/2$

Tanaka et al. (2008) developed a valveless micropump with a diffuser/nozzle shaped channel and a variable volume actuator which produced an oscillating flow. They measured the micropump characteristics for various angles of the microdiffuser ($10° \leq \theta \leq 90°$) and frequencies of the actuator (20 Hz $\leq f \leq$ 140 Hz). Their experimental

results showed that the optimal diffuser/nozzle angle for pump efficiency was $\theta = 50°$. Flow rate increased with increasing the frequency.

Hwang et al. (2008) developed a numerical model using ANSYS to evaluate the flow rate of a reciprocating valveless micropumps. They compared their calculated results with the experimental data with respect to the peak-to-peak voltage (V_{pp}) and the driving frequency (f). Flow rates were measured for different V_{pp} of 150, 175 and 200 V and the driving frequency from 50 to 400 Hz. Experiments were performed three times for each driving condition, from which the mean flow rate and its deviation were evaluated. Their results showed that the driving equivalent moment of the PZT actuation can be used to theoretically analyze the flow characteristics of the micropumps with PZT discs. The frequency for the maximum flow rate was found to be 225 Hz for all V_{pp}. This was slightly different from that by the theoretical calculation of 190 Hz by around 35 Hz. This frequency shift was attributed to stiffening of the PZT disk after the solder bonding for electrical connections. The maximum flow rate was attributed to the most efficient diaphragm–liquid interaction at the corresponding driving frequency. Higher flow rate was achieved with the increase of V_{pp} because of the greater volume oscillation by the larger PZT deformation.

Tsui and Lu (2008) analyzed the flow in a reciprocating valveless micropump using both numerical and lumped-element methods. They modeled the motion of the membrane by imposing a reciprocating velocity boundary condition. They found a good agreement between numerical predictions and experimental data for various back pressure values. They observed a recirculation zone near the entrance corner in the nozzle and another recirculation zone before the fluid enters the nozzle. The former was caused by the sharp entrance while the latter was due to the fact that the recirculation formed by the flow emerging from the microdiffuser in the supply stage persists and moves down toward the central region during the pump stage. The recirculating flow led to a low pressure region at the entrance of the nozzle and thus, caused additional losses. The flow type was reversed in the supply stage. Increasing the back pressure resulted in a decrease in diffuser efficiency.

Experimental investigations of the unsteady flow in a microdiffuser were performed by Sheen et al. (2008). They measured the transient flow behavior in an obstacle-type valveless PZT micropump using a micro-PIV for excitation frequencies in the range $1\ \text{kHz} \leq f \leq 3\ \text{kHz}$. They observed and quantified the flow recirculation around the obstacle, and concluded that such flow behaviors could enhance the flow rectification capability. They observed the phase-shifts between the sectional mean velocities and the excitation voltages when $Wo > 1$. The pressure losses induced by the recirculation regions were direction-dependent. The evolution of the flow recirculation indicated that the obstacle-type valve provided more flow resistances in the reverse flow direction. This flow phenomenon enhanced the flow-directing capability of the obstacle-type valve. For their proposed micropump, the maximum output volume flow rate appeared at the resonance frequency of 1.9 kHz, at which the highest instantaneous velocity was also measured. The volume flow rate increased linearly with the voltages from 15 to 40 V at the resonance frequency.

Nabavi and Mongeau (2009) simulated the high frequency ($10\ \text{kHz} \leq f \leq 30\ \text{kHz}$) pulsating flows through microdiffusers for different divergence angles and maximum pressure amplitudes. This range of frequency is used in valveless acoustic micropump in order to keep the chamber length small ($L_{min} = \lambda/4$). The time-dependent pressures and average velocities at the microdiffuser inlet are shown in Fig. 10 for $\theta = 15°$, at high frequency ($f = 10{,}000$ Hz, left pane) and low frequency ($f = 100$ Hz, right pane). As observed, the time-variant mean velocities are not symmetric, although the pressure variations are symmetric. The mean velocities in the diffuser direction (positive cycles) are larger than those in the nozzle direction (negative cycles). This is due to a lower flow resistance in the diffuser than in the nozzle direction. The phase difference between pressure and velocity signals at high

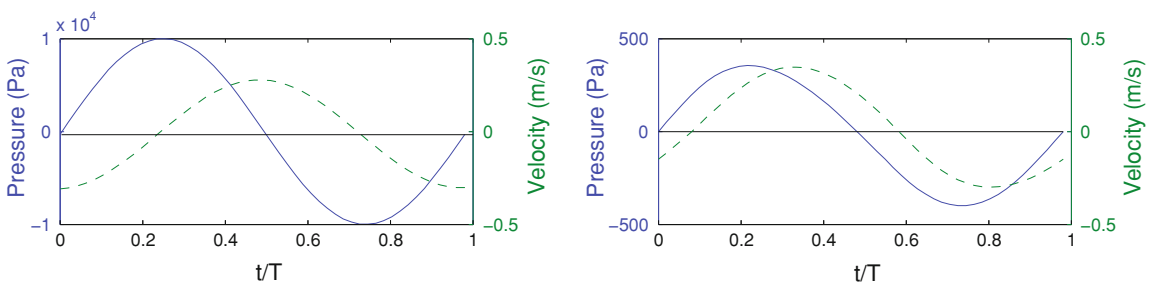

Fig. 10 The time-dependent pressure (*solid line*) and mean velocity (*dashed line*) in a planar microdiffuser with $\theta = 15°$ at high frequency ($f = 10{,}000$ Hz, $P = 10{,}000$ Pa, *left pane*) and low frequency ($f = 100$ Hz, $P = 400$ Pa, *right pane*)

frequency is almost $\pi/2$, contrary to the low frequency case, where the phase difference is considerably less than $\pi/2$ (see Fig. 10). This is due to the fact that at high frequencies the flow impedance ($Z = \frac{\Delta P}{Q} = R + i\omega I$,) is almost purely inductive, and the effect of flow resistance, R, on Z is almost negligible. Whereas, at low frequencies, due to smaller value of ω, both flow resistance (R) and flow inductance (I) contribute in Z. According to Nabavi and Mongeau (2009), the following conclusions can be drawn: flow separation is observed for both high and low frequency cases. However, for low frequency cases, flow separation occurs before the inlet pressure signal changed sign, whereas for high frequency cases, the onset of flow separation coincides with the maximum and minimum of the inlet pressure signal. The life time and size of the flow circulation for the high frequency cases are smaller than those for the low frequency cases. As for low frequencies, better pumping action is found for microdiffuser with larger divergence angles at high excitation frequencies. Increase of maximum pressure or decrease of excitation frequency results in increase of net flow rate and rectification capability. The values of flow resistance, inductance, and impedance in diffuser direction are lower than those in nozzle direction. The values of R_d, I_d, Z_d, R_n, I_n, and Z_n decrease as θ increases. An increase in f or a decrease in P causes an increase in R_d and I_d, and a decrease in R_n, I_n, and consequently an decrease in net velocity and rectification capability. For the same amount of net flow rate, the total amount of energy losses over one cycle for low frequency case is greater than that for the high frequency case. This is due to the lower size and life time of flow circulation at low frequency compared to high frequency.

6.1 Effects of different design parameters

Based on the above-mentioned studies, microdiffusers and micropumps show different performances at different design parameters or working conditions in the unsteady flow regime. A summary of the effects of these parameters on the performance of microdiffusers and micropumps is provided in the following:

1. Effects of Reynolds number:
   - For planar microdiffusers, η increases with increasing Re, regardless the diffuser angle (Sun and Huang 2006; Wang et al. 2007; Nabavi and Mongeau 2009). This is in contradiction with the results of the steady flow regime where η decreases with increasing Re.
   - For the total pump, net flow rate increases with increasing Re, regardless the diffuser angle (Tanaka et al. 2008; Sheen et al. 2008; Hwang et al. 2008).
2. Effects of diffuser angle:
   - For planar microdiffusers, both ξ_n and ξ_d decrease with increasing θ, regardless the Reynolds number (Sun and Huang 2006). This is in agreement with the results of the steady flow regime.
   - For planar microdiffusers, η increases with increasing θ, regardless the Reynolds number (Sun and Huang 2006; Nabavi and Mongeau 2009). This is in contradiction with the results of the steady flow regime.
   - For the total pump, maximum net flow rate is achieved at a critical value of θ (Tanaka et al. 2008).
3. Effects of excitation frequency:
   - For planar microdiffusers, η is independent of f for small frequencies, and then decreases with increasing f, regardless the Reynolds number (Sun and Huang 2006; Wang et al. 2007; Nabavi and Mongeau 2009).
   - For the total pump, The net flow rate increases with increasing f up to a critical frequency (f_{cr}), and decreases with further increase of frequency beyond f_{cr} (Sheen et al. 2008; Hwang et al. 2008).
   - Flow rate is approximately in phase with pressure at low frequencies, but phase shift ascends as actuation frequency is increased. It reaches $\pi/2$ at very high frequencies (Sun and Huang 2006; Ahmadian et al. 2006; Nabavi and Mongeau 2009).
4. Flow separation:
   - In the unsteady flow regime, flow separation is inevitable for microdiffusers regardless of its angle, excitation frequency and corresponding Reynolds number. The size and life time of flow separation increase with increasing θ (Sun and Huang 2006; Nabavi and Mongeau 2009).
   - At low frequencies, flow separation occurs before the inlet pressure signal changed sign (Sun and Huang 2006). However, for high frequency cases, the onset of flow separation coincides with the maximum and minimum of the inlet pressure signal (Nabavi and Mongeau 2009).
   - The life time and size of the flow recirculation region for the low frequency cases is larger than those for the high frequency cases. According to Nabavi and Mongeau (2009), at $f = 10{,}000$ Hz, flow separation occurs at 12% and 16% of the period for $\theta = 15°$ and 45°, respectively. For $f = 100$ Hz, these values are 30% and 42% for $\theta = 15°$ and 45°, respectively.

Figure 11 shows the typical shape of flow field inside the microdiffuser in the unsteady flow regime at low ($f = 100$ Hz) and high ($f = 10{,}000$ Hz) frequencies. The figure clearly shows that size of the flow recirculation region for the low frequency case is larger than that for the high frequency case.

7 Flow visualization in micropumps

The velocity field in the reciprocating valveless micropumps is pulsatile and composed of a periodical oscillating flow component superimposed on a steady flow component (see velocity waveforms in Fig. 10). Visualization of pulsating flow poses many significant measurement challenges. For example, in pulsating flow, the measuring instrument should be synchronized with the characteristic of the flow which is not required for steady flow measurements. Some of the macroscopic measurement techniques, such as, particle image velocimetry (PIV), laser Doppler velocimetry (LDV), and scalar image velocimetry (SIV) were modified for micro-scale applications (Sinton 2004; Lee and Kim 2009). Among these techniques, micro-PIV has been widely used for flow visualization in microdiffusers and micropumps.

Micro-PIV measurement of instantaneous velocity fields is a challenging task. Some of these challenges are: (1) when the seed particles are very small, collisions between the fluid molecules and seed particles result in random motion of particles. This phenomenon, called *Brownian motion*, causes an error in the measurement of the flow velocity. (2) In macroscopic PIV, the measurement plane is defined by a laser sheet illuminating the desired segment of the flow. In micro-PIV, however, because of the small dimensions of the fluidic channels, the volume-illumination is applied. Volume-illumination allows particles within an image depth to contribute to the correlation and the measurement is a weighted average of the flow within the depth of correlation. For relatively large correlation depths, this may result in distortion of the correlation peak and significant measurement errors. (3) The seed particles should be small enough to track the flow faithfully, but at the same time, they must be large enough to dampen the effects of Brownian motion, and to provide sufficient scatter light. For gas flows, the challenge of seeding particles suitable for microfluidic devices is more severe. (4) In general, the particle images obtained by micro PIV have low signal-to-noise ratios because sub-micron particles do not emit sufficient intensity to be recorded. Hence, basic PIV algorithms yield many error vectors. Therefore, some advanced PIV algorithms which are capable of providing a reasonable vector even in regions with poor image quality should be employed.

Micro-PIV system consists of an Nd:YAG laser, a CCD camera, a timer box, optics, and a computer equipped with a frame grabber. For micro-PIV measurement, fluorescent particles of submicron size are commonly used instead of tracer particles. The sampling rate of conventional micro-PIV systems is 15 Hz, which is much lower than the excitation frequency of the micropump. Therefore, a synchronizer that synchronize the laser pulses and camera frames with the excitation signal is required for pulsating velocity measurements (Nabavi et al. 2007b). This feature makes it possible to investigate not only sinusoidal pulsations, but also any kind of periodic and non-periodic variations experimentally. Several images can be acquired and processed for each particular phase to increase the signal-to-noise ratio.

Sheen et al. (2008) used a synchronized micro-PIV to visualize flow fields at the outlet and around the obstacle of an obstacle-type valveless micropump, at various phases of the excitation signal with the frequency range between 1 and 3 kHz. They chose fluorescent particles (diameter 700 nm) with an excitation peak at 542 nm and emission peak at 612 nm as the tracer particles. The camera field of view was 500 μm × 500 μm. A longer time interval was chosen for lower instantaneous flow velocity to reduce Brownian errors. A suitable adjustment of time interval (between 5 and 200 μs) was performed in the measurement. The Brownian error was thus controlled to be less than 1% for all results in a cycle. The response time of a 700 nm particle was calculated to be less than 10^{-7} s, which was far shorter than the cycling period. The particle sizes were less than 1% of the hydraulic diameter of the channel. They concluded that, in the profiles at the outlet, maximum velocity no longer appeared in the central region, but close to the side-wall. The time-dependent distributions consistently showed a decrease of velocity from the boundary layer to the central region. These phenomena were apparently observed when the pump and

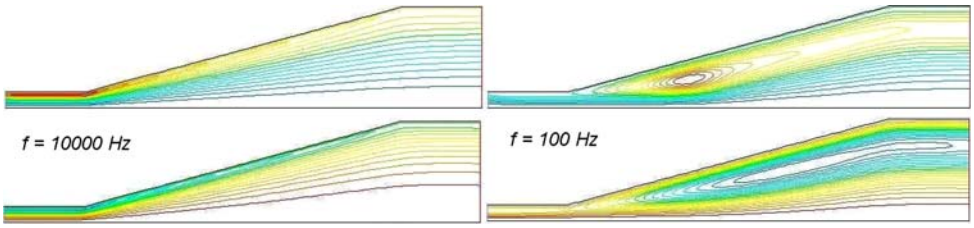

Fig. 11 Typical flow field inside the planar microdiffuser in unsteady flow regime at low (100 Hz) and high (10,000 Hz) frequencies

supply phases were switched. The flow recirculation around the obstacle was also observed and quantified to investigate the influence on the pump performance. The duration, circulation, and the size of the recirculation regions indicated that this flow behavior could enhance the flow-directing capability.

Hsu and Sheen (2008) used a synchronized micro-PIV system to investigate the performance of a double-chamber planar micropump that could work in the in-phase and anti-phase modes. The flow measurements using micro-PIV clearly demonstrated the process of how oscillatory flows were converted into a smoothly continuous flow in anti-phase mode operation. Based on flow rectifying capability and conversion ratio, the pumping performance and flow quality were found to possess optimal values when the operation frequencies were in the range of 0.2–0.8 kHz.

8 Concluding remarks

In the present review, a brief summary of the latest micropump technologies along with the advantages and disadvantages of each mechanism with the emphasis on the innovative and less-reviewed valveless micropumps are provided. The non-mechanical passive microvalves as part of valveless micropumps are then described. Piezoelectric micropumps with fixed microvalves which are the most-investigated type of micropumps are reviewed. The more important objective of this review is to survey the recent numerical and experimental studies on the steady and pulsating flows through different types of microdiffusers and valveless micropumps. A comprehensive review of the effects of different design parameters on the performance of microdiffusers and valveless micropumps in both steady and unsteady flow regimes is provided. Quantitative comparisons of different steady and unsteady studies are also provided in tabular forms. The challenges and applications of micro-PIV measurement of pulsatile flow through microdiffusers and valveless micropumps are discussed.

Based on the studies reviewed in this paper, the following differences between the performance of microdiffusers and micropumps in steady and unsteady flow regimes can be drawn:

- For planar microdiffusers regardless the diffuser angle, η decreases with increasing Re in the the steady flow regime. Whereas, η increases with increasing Re in the the unsteady flow regime.
- In valveless micropumps with planar microdiffusers in the steady flow regime, the net flow rate is maximized at a critical value of θ, and decreases with increasing or decreasing θ from this value. However, in the unsteady flow regime, the net flow rate increases exponentially with increasing θ.
- With the same Re and diffuser shape and angle, the overall net flow rate of the valveless micropump in the steady flow regime is higher than that in the unsteady flow regime.
- In the unsteady flow regime, flow separation is observed in microdiffuser, regardless of its angle, and Reynolds number. Whereas, in the steady flow regime, for small values of θ, there is no flow separation in the microdiffuser, and as θ increases beyond a critical value, separation occurs.

Performing numerical and experimental investigations of the steady flow in microdiffusers and micropumps is easier than that of the unsteady flow, and may be used for the design of diffuser micropumps at low frequencies. However, the unsteadiness of the flow affects the performance of the microdiffusers and micropumps and degrade the accuracy of the steady analysis at higher frequencies. On the other hand, unsteady numerical and experimental investigations provide more accurate results. However, performing experiments and simulations in unsteady flow regime is more difficult.

Based on an extensive literature review, it is concluded that there are still many possible areas of research in the field of steady and unsteady flows through microdiffusers and micropumps. There are some inconsistences and contradictions regarding the effect of some parameters on the performance of microdiffusers and micropumps, which need to be resolved, for example, the effects of θ and Re on the efficiency of microdiffusers in steady flow regime. Furthermore, the effects of some parameters, such as, slenderness of microdiffuser, surface roughness, temperature, density and viscosity of the working fluid, shape of entrance and exit sections of microdiffuser, etc. have not been investigated. Some comprehensive experimental or experimentally validated numerical studies that investigate the effects of any one parameter while the other parameters are kept unchanged, are needed. All the important design parameters, such as, shape, angle, area ratio, length and slenderness of microdiffuser, Reynolds number, frequency, type of working fluid, and back pressure should be included in such studies.

Previous studies involve Newtonian fluids, mostly water. However, micropump should work with some biofluids which are non-Newtonian fluids. Understanding the performance of microdiffusers and micropumps with non-Newtonian fluids is an important step towards realization of micropumps. Another significant research area that needs extensive investigation is flow control of micropumps. It would be useful to work on some linear,

nonlinear and adaptive control mechanisms to adjust some parameters, such as, vibrating amplitude and frequency of the actuator in order to control the flow rate of the micropumps.

Acknowledgments This research was funded by grants from the Fonds Québécois de Recherche sur la Nature et les Technologies (FQRNT).

References

Ahmadian M, Saidi M, Mehrabian A, Bazargan M, Kenarsari S (2006) Performance of valveless diffuser micropumps under harmonic piezoelectric actuation. In: ASME Conference on engineering systems design and analysis

Amirouche F, Zhou Y, Johnson T (2009) Current micropump technologies and their biomedical applications. Microsyst Technol 15:647–666

Andersson H, van der Wijngaart W, Nilsson P, Enoksson P, Stemme G (2001) A valve-less diffuser micropump for microfluidic analytical systems. Sens Actuators B 72:259–265

Bae B, Kim N, Kee H, Kim S, Lee Y, Lee S, Park K (2002) Feasibility test of an electromagnetically driven valve actuator for glaucoma treatment. J Microelectromech Syst 11:344–354

Bennett M, Leo D (2004) Ionic liquids as stable solvents for ionic polymer transducers. Sens Actuators A 115:79–90

Brufau-Penella J, Tsiakmakis K, Laopoulos T, Puig-Vidal M (2008) Model reference adaptive control for an ionic polymer metal composite in underwater applications. Smart Mater Struct 17:045–020

Cecchini M, Girardo S, Pisignano D, Cingolani R, Beltram F (2008) Acoustic-counterflow microfluidics by surface acoustic waves. Appl Phys Lett 92:104–103

Chen Y, Kang S, Wu L, Lee S (2008) Fabrication and investigation of pdms micro-diffuser/nozzle. J Mater Process Technol 198:478–484

Cheng H, Chien C (2008) Ejection characteristics of micropumps for motorcycle fuel atomizer in high-temperature environment. Appl Therm Eng 28:94–109

Cui Q, Liu C, Zha X (2007) Study on a piezoelectric micropump for controlled drug delivery system. Microfluid Nanofluid 3:377–390

Cui Q, Liu C, Zha X (2008) Simulation and optimization of a piezoelectric micropump for medical applications. Int J Adv Manuf Technol 36:516–524

Dario P, Crocey N, Carrozzay M, Varalloz G (1996) A fluid handling system for a chemical microanalyzer. J Micromech Microeng 6:95–98

Dario P, Carrozza M, Benvenuto A, Menciassi A (2000) Micro-systems in biomedical applications. J Micromech Microeng 10:235–244

da Silva A, Kobayashi M, Coimbra C (2007) Optimal theoretical design of 2-D microscale viscous pumps for maximum mass flow rate and minimum power consumption. Int J Heat Fluid Flow 28:526–536

Deshpande M, Gilbert J, Bardell R, Forster F (1998) Design analysis of no-moving-parts valves for micropumps. J Microelectromech Syst DSC 66:153–158

Dopper J, Clemens M, Ehrfeld W, Jung S, Kamper K, Lehr H (1997) Micro gear pumps for dosing of viscous fluids. J Micromech Microeng 7:230–232

Du X, Swanwick M, Fu Y, Luo J, Flewitt A, Lee D, Maeng S, Milne W (2009) Surface acoustic wave induced streaming and pumping in 128° y−cut $LiNbo_3$ for microfluidic applications. J Micromech Microeng 19:035–016

Ehlert S, Hlushkou D, Tallarek U (2008) Electrohydrodynamics around single ion-permselective glass beads fixed in a microfluidic device. Microfluid Nanofluid 4:471–487

Erickson D (2005) Towards numerical prototyping of labs-on-chip: modeling for integrated microfluidic devices. Microfluid Nanofluid 1:301–318

Fair R (2007) Digital microfluidics: is a true lab-on-a-chip possible? Microfluid Nanofluid 3:245–281

Fan B, Song G, Hussain F (2005) Simulation of a piezoelectrically actuated valveless micropump. Smart Mater Struct 14:400–405

Feldt C, Chew L (2002) Geometry-based macro-tool evaluation of non-moving-part valvular microchannels. J Micromech Microeng 12:662–669

Forster F, Bardell R, Afromowitz M, Sharma N, Blanchard A (1995) Design, fabrication and testing of fixed-valve micro-pumps. In: Proceedings of the ASME fluids engineering division

Forster F, Bardell R, Sharma N (2001) Methods for making micropumps. US Patent 6227809 B1

Garimella S, Singhal V, Liu D (2006) On-chip thermal management with microchannel heat sinks and integrated micropumps. Proc IEEE 94:1534–1548

Gerlach T (1998) Microdiffusers as dynamic passive valves for micropump applications. Sens Actuators A 69:181–191

Gerlach T, Schuenemann M, Wurmus H (1995) A new micropump principle of the reciprocating type using pyramidic micro flowchannels as passive valves. J Micromech Microeng 5:199–201

Guttenberg Z, Rathgeber A, Keller S, Rädler J, Wixforth A, Kostur M, Schindler M, Talkner P (2004) Flow profiling of a surface-acoustic-wave nanopump. Phys Rev E 70:056–311

Haik Y, Kilani M, Hendrix J, Rifai O, Galambos P (2007) Flow field analysis in a spiral viscous micropump. Microfluid Nanofluid 3:527–535

Hsieh S, Lin C, Huang C, Tsai H (2004) Liquid flow in a micro-channel. J Micromech Microeng 14:436–445

Hsu Y, Le N (2008) Equivalent electrical network for performance characterization of piezoelectric peristaltic micropump. Microfluid Nanofluid. doi:101007/s10404-008-0380-7

Hsu C, Sheen H (2008) A microfluidic flow-converter based on a double-chamber planar micropump. Microfluid Nanofluid. doi:101007/s10404-008-0347-8

Hsu Y, Lin S, Hou S (2007) Development of peristaltic antithrombogenic micropumps for in vitro and ex vivo blood transportation tests. Microsyst Technol 14:31–41

Hu J, Tan C, Hu W (2007a) Ultrasonic microfluidic transportation based on a twisted bundle of thin metal wires. Sens Actuators A 135:811–817

Hu Y, Xuan X, Werner C, Li D (2007b) Electroosmotic flow in microchannels with prismatic elements. Microfluid Nanofluid 3:151–160

Hwang I, An J, Ko K, Shin S, Lee J (2007) A novel micropump with fixed-geometry valves and low leakage flow. J Micromech Microeng 17:1632–1639

Hwang I, Lee S, Shin S, Lee Y, Lee J (2008) Flow characterization of valveless micropump using driving equivalent moment: theory and experiments. Microfluid Nanofluid 5:795–807

Iverson B, Garimella S (2008) Recent advances in microscale pumping technologies: a review and evaluation. Microfluid Nanofluid. doi:101007/s10404-008-0266-8

Izzo I, Accoto D, Menciassi A, Schmitt L, Dario P (2007) Modeling and experimental validation of a piezoelectric micropump with novel no-moving-part valves. Sens Actuators A 133:128–140

Jang L, Kan W (2007) Peristaltic piezoelectric micropump system for biomedical applications. Biomedical Microdevices 9:619–626

Jang L, Yu Y (2008) Peristaltic micropump system with piezoelectric actuators. Microsyst Technol 14:241–248
Jeong J, Kim C (2007) A numerical simulation on diffuser-nozzle based piezoelectric micropumps with two different numerical models. Int J Numer Methods Fluids 53:561–571
Jiang X, Zhou Z, Huang X, Li Y, Yang Y, Liu C (1998) Micronozzle/diffuser flow and its application in micro valveless pumps. Sens Actuators A 70:81–87
Jiang L, Mikkelsen J, Koo J, Huber D, Yao S, Zhang L, Zhou P, Maveety J, Prasher R, Santiago J, Kenny T, Goodson K (2002) Closed-loop electroosmotic microchannel cooling system for VLSI circuits. IEEE Trans Compon Packag Technol 25:347–355
Junwu K, Zhigang Y, Taijiang P, Guangming C, Boda W (2005) Design and test of a high-performance piezoelectric micropump for drug delivery. Sens Actuators A 121:156–161
Koch M, Evans A, Brunnschweiler A (1998) The dynamic micropump driven with a screen printed PZT actuator. J Micromech Microeng 8:119–122
Kohl M, Abdel-Khalik S, Jeter S, Sadowski D (2005) An experimental investigation of microchannel flow with internal pressure measurements. Int J Heat Mass Transf 48:1518–1533
Laser D, Santiago J (2004) A review of micropumps. J Micromech Microeng 14:r35–r64
LaVan D, McGuire T, Langer R (2003) Small-scale systems for in vivo drug delivery. Nat Biotechnol 21:1184–1191
Lee J, Li D (2006) Electroosmotic flow at a liquid–air interface. Microfluid Nanofluid 2:361–365
Lee S, Kim S (2009) Advanced particle-based velocimetry techniques for microscale flows. Microfluid Nanofluid 6:577–588
Li H, Roberts D, Steyn J, Turner K, Yaglioglu O, Hagood N, Spearing S, Schmidt M (2004) Fabrication of a high frequency piezoelectric microvalve. Sens Actuators A 111:51–56
Li B, Chen Q, Lee D, Woolman J, Carman G (2005) Development of large flow rate, robust, passive micro check valves for compact piezoelectrically actuated pumps. Sens Actuators A 117:325–330
Lien K, Liu C, Lin Y, Kuo P, Lee G (2008) Extraction of genomic dna and detection of single nucleotide polymorphism genotyping utilizing an integrated magnetic bead-based microfluidic platform. Microfluid Nanofluid. doi:101007/s10404-008-0337-x
Ma B, Liu S, Gan Z, Liu G, Cai X, Zhang H, Yang Z (2006) A pzt insulin pump integrated with a silicon microneedle array for transdermal drug delivery. Microfluid Nanofluid 2:417–423
Ma H, Chen B, Lin C, Gao J (2008) The improved performance of one-side actuating diaphragm micropump for a liquid cooling system. Int Commun Heat Mass Transf 35:957–966
Ma H, Chen B, Gao J, Lin C (2009) Development of an OAPCP-micropump liquid cooling system in a laptop. Int Commun Heat Mass Transf 36:225–232
Machauf A, Nemirovsky Y, Dinnar U (2005) A membrane micropump electrostatically actuated across the working fluid. J Micromech Microeng 15:2309–2316
Mala G, Li D (1999) Flow characteristics of water in microtubes. Int J Heat Fluid Flow 20:142–148
Maruo S, Inoue H (2007) Optically driven viscous micropump using a rotating microdisk. Appl Phys Lett 91:084101
Morris C, Forster F (2000) Optimization of a circular piezoelectric bimorph for a micropump driver. J Micromech Microeng 10:459–465
Morris C, Forster F (2003) Low-order modeling of resonance for fixed-valve micropumps based on first principles. J Microelectromech Syst 12:325–334
Mugele F, Baret J (2005) Electrowetting: from basics to applications. J Phys Condens Matter 17:705–774
Nabavi M, Mongeau L (2009) Numerical analysis of high frequency pulsating flows through a diffuser-nozzle element in valveless acoustic micropumps. Microfluid Nanofluid. doi:101007/s10404-009-0427-4
Nabavi M, Siddiqui K, Dargahi J (2007a) A new 9-point sixth-order accurate compact finite difference method for the Helmholtz equation. J Sound Vib 307:972–982
Nabavi M, Siddiqui K, Dargahi J (2007b) Simultaneous measurement of acoustic and streaming velocities using the synchronized PIV technique. Meas Sci Technol 18:1811–1817
Nabavi M, Siddiqui K, Dargahi J (2008a) Analysis of the flow structure inside the valveless standing wave pump. Phys Fluids 20:126101
Nabavi M, Siddiqui K, Dargahi J (2008b) A fourth-order accurate scheme for solving one-dimensional highly nonlinear standing wave equation in different thermoviscous fluids. J Comput Acoust 16:563–576
Nguyen B, Kassegne S (2008) High-current density dc magenetohydrodynamics micropump with bubble isolation and release system. Microfluid Nanofluid 5:383–393
Ogawa J, Kanno I, Kotera H, Wasa K, Suzuki T (2009) Development of liquid pumping devices using vibrating microchannel walls. Sens Actuators A 152:211–218
Oh K, Ahn C (2006) A review of microvalves. J Micromech Microeng 16:R13–R39
Olsson A, Stemme G, Stemme E (1995) A valve-less planar fluid pump with two pump chambers. Sens Actuators A 46:549–556
Olsson A, Enoksson P, Stemme G, Stemme E (1996a) A valve-less planar pump isotropically etched in silicon. J Micromech Microeng 6:87–91
Olsson A, Stemme G, Stemme E (1996b) Diffuser-element design investigation for valve-less pumps. Sens Actuators A 57:137–143
Olsson A, Stemme G, Stemme E (1999) A numerical design study of the valveless diffuser pump using lumped-mass model. J Micromech Microeng 9:34–44
Olsson A, Stemme G, Stemme E (2000) Numerical and experimental studies of flat-walled diffuser elements for valve-less micropumps. Sens Actuators A 84:165–175
Pal R, Yang M, Johnson B, Burke D, Burns M (2004) Phase change microvalve for integrated devices. Anal Chem 76:3740–3748
Pan L, Ng T, Liu G, Lam K, Jiang T (2001) Analytical solution for the dynamic analysis of a valveless micropump: a fluid-membrane coupling study. Sens Actuators A 93:173–181
Park H, Lim J (2008) A reduced-order model of the low-voltage cascade electroosmotic micropump. Microfluid Nanofluid. doi:101007/s10404-008-0326-0
Park J, Yoshida K, Yokota S (1999) Resonantly driven piezoelectric micropump fabrication of a micropump having high power density. Mechatronics 9:687–702
Paul B, Terhaar T (2000) Comparison of two passive microvalve designs for microlamination architectures. J Micromech Microeng 10:15–20
Peng X, Peterson G, Wang B (1994) Heat transfer charactheristics of water flowing through microchannels. Exp Heat Transf 7:265–283
Renaudin A, Tabourier P, Zhang V, Camart J, Druon C (2006) SAW nanopump for handling droplets in view of biological applications. Sens Actuators B 113:389–397
Rich C, Wise K (2003) A high-flow thermopneumatic microvalve with improved efficiency and integrated state sensing. J Microelectromech Syst 12:201–208
Schabmueller C, Koch M, Mokhtari M, Evans A, Brunnschweiler A, Sehr H (2002) Self-aligning gas/liquid micropump. J Micromech Microeng 12:420–424
Seibel K, Schler L, SchSfer H, Bhm M (2008) A programmable planar electroosmotic micropump for lab-on-a-chip applications. J Micromech Microeng 18:025008

Sen M, Wajerski D, el Hak MG (1996) A novel pump for MEMS applications. J Fluids Eng 118:624–627
Sharatchandra M, Sen M, el Hak MG (1997) Navier stokes simulations of a novel viscous pump. J Fluids Eng 119:372–382
Sheen H, Hsu C, Wu T, Chu H, Chang C, Lei U (2007) Experimental study of flow characteristics and mixing performance in a PZT self-pumping micromixer. Sens Actuators A 139:237–244
Sheen H, Hsu C, Wu T, Chang C, Chu H, Yang C, Lei U (2008) Unsteady flow behaviors in an obstacle-type valveless micropump by micro-PIV. Microfluid Nanofluid 4:331–342
Shoji S, Esashi M (1994) Microflow devices and systems. J Micromech Microeng 4:157–171
Singhal V (2007) Micropump for electronics cooling. US Patent 20070020124
Singhal V, Garimella S, Murthy J (2004) Low reynolds number flow through nozzle/diffuser elements in valveless micropumps. Sens Actuators A 113:226–235
Sinton D (2004) Microscale flow visualization. Microfluid Nanofluid 1:2–21
Stemme E, Stemme G (1993) A valveless diffuser/nozzle-based fluid pump. Sens Actuators A 39:159–167
Sun C, Huang K (2006) Numerical characterization of the flow rectification of dynamic microdiffusers. J Micromech Microeng 16:1331–1339
Sun C, Yang Z (2007) Effects of the half angle on the flow rectification of a microdiffuser. J Micromech Microeng 17:2031–2038
Suzuki H, Yoneyama R (2003) Integrated microfluidic system with electrochemically actuated on-chip pumps and valves. Sens Actuators B 96:38–45
Tabak A, Yesilyurt S (2007) Numerical simulations and analysis of a micropump actuated by traveling plane waves. Microfluidics BioMEMS and Medical Microsystems V. doi:101117/12702320
Tanaka S, Tsukamoto H, Miyazaki K (2008) Development of diffuser/nozzle based valveless micropump. J Fluid Sci Technol 3:999–1007
Tesla E (1920) Valvular conduit. US Patent 1,329,559
Teymoori M, Abbaspour-Sani E (2005) Design and simulation of a novel electrostatic peristaltic micromachined pump for drug delivery applications. Sens Actuators A 117:222–229
Tsui Y, Lu S (2008) Evaluation of the performance of a valveless micropump by CFD and lumped-system analyses. Sens Actuators A 148:138–148
Verma P, Chatterjee D, Nagarajan T (2009) Design and development of a modular valveless micropump on a printed circuit board for integrated electronic cooling. J Mech Eng Sci 223:953–963
Wang B, Chu X, Li E, Li L (2006) Simulations and analysis of a piezoelectric micropump. Ultrasonics 44:e643–e646
Wang C, Leu T, Sun J (2007) Unsteady analysis of microvalves with no moving parts. J Mech 23:9–14
Wang Y, Kang Y, Xu D, Barnett L, Kalams S, Li D, Li D (2008) On-chip total counting and percentage determination of CD4+Tlymphocytes. Lab-Chip 8:309–315
Wang Y, Hsu J, Kuo P, Lee Y (2009) Loss characteristics and flow rectification property of diffuser valves for micropump applications. Int J Heat Mass Transf 52:328–336
Wiederkehr R, Salvadori M, Brugger J, Degasperi F, Cattani M (2008) The gas flow rate increase obtained by an oscillating piezoelectric actuator on a micronozzle. Sens Actuators A 144:154–160
Woias P (2005) Micropumps: past, progress and future prospects. Sens Actuators B 105:28–38
Wu J, Ben Y, Chang H (2005) Particle detection by electrical impedance spectroscopy with asymmetric-polarization ac electroosmotic trapping. Microfluid Nanofluid 1:161–167
Yamaguchi N, Yang M (2004) Development and evaluation of a micro chemical gas sensor with an inner-circulation diffuser pump. Sens Actuators B 103:369–374
Yamahata C, Chastellain M, Parashar V, Petri A, Hofmann H, Gijs M (2005a) Plastic micropump with ferrofluidic actuation. J Microelectromech Syst 14:94–102
Yamahata C, Lacharme F, Burri Y, Gijs M (2005b) A ball valve micropump in glass fabricated by powder blasting. Sens Actuators B 110:1–7
Yamahata C, Lotto C, Al-Assaf E, Gijs M (2005c) A PMMA valveless micropump using electromagnetic actuation. Microfluid Nanofluid 1:197–207
Yang K, Chen I, Wang BSC (2004a) Investigation of the flow characteristics within a micronozzle/diffuser. J Micromech Microeng 14:26–31
Yang X, Holke A, Jacobson S, Lang J, Schmidt A, Umans S (2004b) An electrostatic, on/off microvalve designed for gas fuel delivery for the mit microengine. J Microelectromech Syst 13:660–668
Yang Y, Hsiung S, Lee G (2008) A pneumatic micropump incorporated with a normally closed valve capable of generating a high pumping rate and a high back pressure. Microfluid Nanofluid. doi:101007/s10404-008-0356-7
Yao Q, Xu D, Pan L, Teo A, Ho W, Lee V, Shabir M (2007) CFD simulations of flows in valveless micropumps. Eng Appl Comput Fluid Mech 1:181–188
Yoshida H (2005) The wide variety of possible applications of microthermofluid control. Microfluid Nanofluid 1:289–300
Yoshida K, Kikuchi M, Park J, Yokota S (2002) Fabrication of micro electro-rheological valves (ER valves) by micromachining and experiments. Sens Actuators A 95:227–233
Zhang T, Wang Q (2005) Valveless piezoelectric micropump for fuel delivery in direct methanol fuel cell (DMFC) devices. J Power Sources 140:72–80
Zhang T, Wang Q (2006) Performance of miniaturized direct methanol fuel cell (DMFC) devices using micropump for fuel delivery. J Power Sources 158:169–176
Zhang C, Xing D, Li Y (2007) Micropumps, microvalves, and micromixers within pcr microfluidic chips: advances and trends. Biotechnol Adv 25:483–514